Theme IIIc: Thin-walled metal shells

III c
Coques métalliques
Stahl- und Leichtmetallschalen
Thin-Walled Metal Shells

Leere Seite
Blank page
Page vide

Stability of Thin-Steel Hyperbolic Paraboloid Roofs

Stabilité de toitures minces en acier, de forme paraboloide hyperbolique

Stabilität dünner hyperbolischer Paraboloid-Stahldächer

PETER GERGELY
Structural Engineering
Cornell University
USA

Several types of roofs for a variety of structures may be built of thin-steel hyperbolic paraboloid (hypar) units. The basic unit of such roofs is composed of structural steel or thin-steel edge members and of a warped surface made of thin (light gage) steel panels [1]. Attractive roofs can be constructed by various combinations of these units. The resulting structure has high strength to weight ratio. Some aspects of metal hypar structures have been described by the theme reporter, Monsieur P. A. Lorin.

A remarkable example is shown in Fig. 1. This hangar,

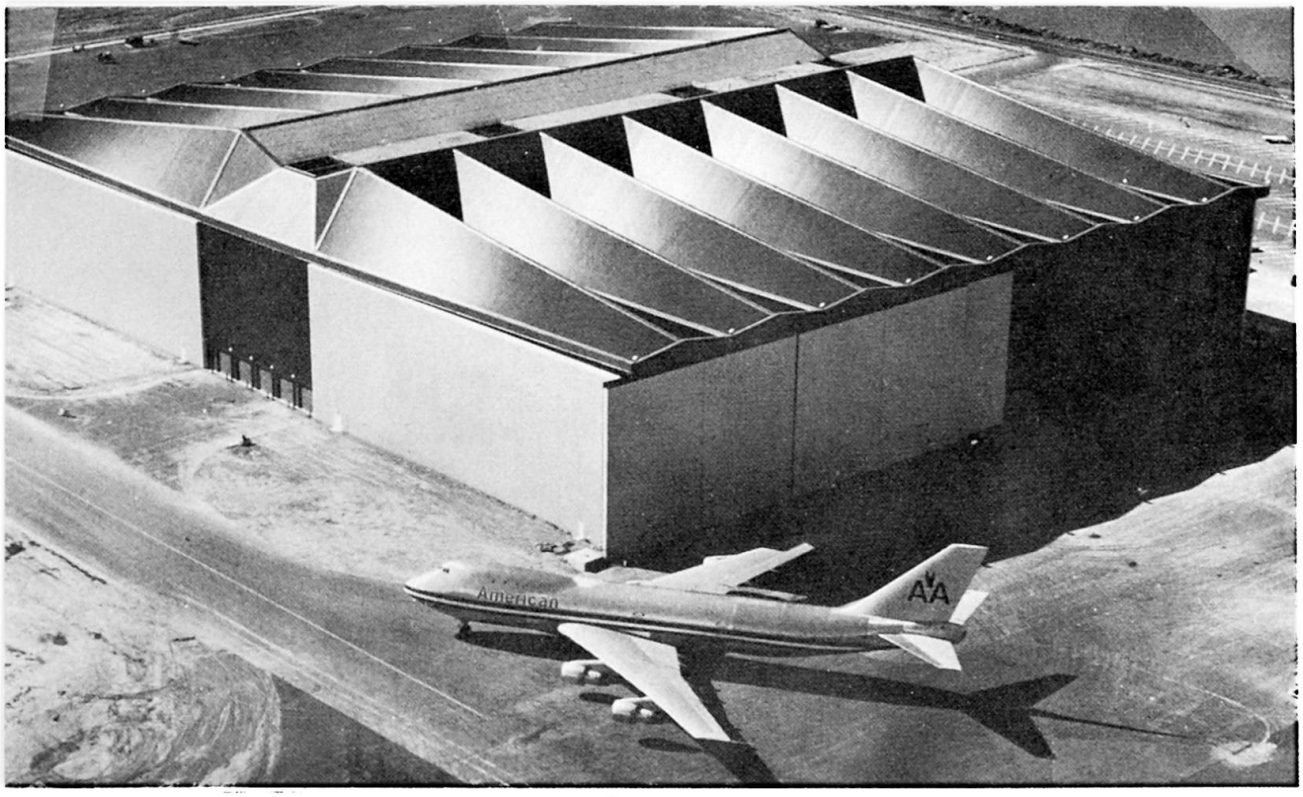

Fig. 1

designed by Lev Zetlin Associates, New York, N.Y., is covered by 230 ft (70 m) long and 56 ft (17 m) wide thin-steel hypar modules. The depth of these free cantilevers varies from 40 ft (12 m) to 4 ft (1,2 m) to accommodate the largest aircraft.

The key to the success of this type of structures lies in the well demonstrated fact [2, 3] that thin-steel diaphragms can resist in-plane shear forces quite well and that the forces in hypar shells are dominated by membrane shear forces.

Design Problems

The calculation of stresses in thin-steel hypars can usually be estimated using the simple membrane theory. This was demonstrated during an extensive analytical and experimental study at Cornell University. However, design is ordinarily controlled by stiffness (deflection and buckling) considerations.

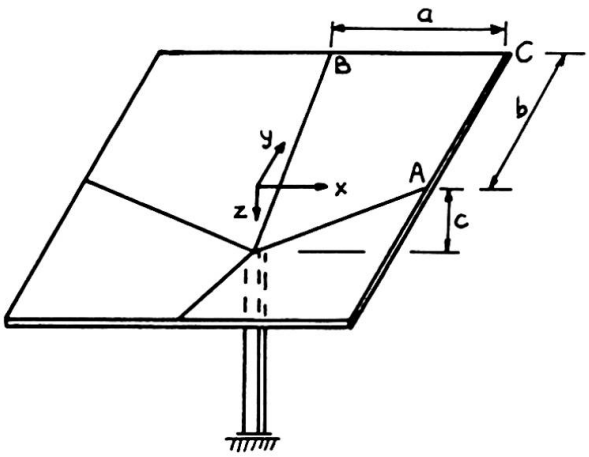

Fig. 2

Deflections may be a problem at flat corners of several types of hypar roofs (such as at the outside corners of the inverted umbrella roof of Fig. 2), or at the center of shallow deck units.

Instability may develop in three ways: a) the deck may buckle under the membrane shear forces, b) the compression edge members may buckle due to the nonconservative force system transmitted by the membrane shear [1], and c) local buckling of the deck may occur. The first and most important type of instability is the subject of this contribution. Edge member buckling was found to be unimportant in well designed structures [3], and local buckling is discussed in detail in papers on diaphragm design.

Deflections and instability depend strongly on the effective shear rigidity of the deck. This quantity is influenced by several factors [2], primarily by the connections between the deck and the edge members and between the panels of the deck, in addition to the geometry of the deck deformations. Frequently two layers of decking, with the corrugations or deformations running in orthogonal directions, are used to increase stiffness and, in some cases, to decrease bending stresses. The second important factor is the curvature (loosely speaking the rise-span ratio) of the structure.

Shell Buckling

The buckling of thin-steel decks is caused by diagonal compressive stresses associated with membrane shear stresses. The situation is very similar to the behavior of thin webs or shear diaphragms. Whereas the stability of isotropic hypar shells with fully supported edges was evaluated explicitly in a classical paper by Reissner [4], the buckling of orthotropic shells is a much more complex matter because of the presence of several rigidities D_x, D_y, D_{xy}, and D_1.

Considering the importance of shell buckling in the design of thin-steel hypar structures, the question was approached from several directions. An experimental study consisted of small and medium-scale model tests. Two analytical methods were developed: a rigorous analysis based on the finite element technique, and an approximate analysis using energy methods.

Experimental Investigation

Several tests were performed on small scale, 12 in. by 12 in. (30 cm by 30 cm) umbrella type hypars with sinusoidal corrugated decking [1]. However, it was difficult to assess the basic properties of the deck, connections, and edge members, and therefore these tests resulted in little quantitative data.

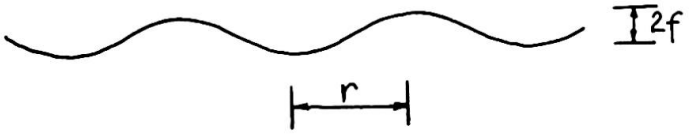

Fig. 3

Four medium-scale, 12 ft by 12 ft (3,65 m by 3,65 m) umbrella type hypars were tested. The decking consisted of one or two layers of standard corrugated sheets (Fig. 3), for which f = 0.25 in. (6,4 mm) and r = 1.33 in. (3,4 cm). The edge members were structural tubing. The decks were attached with #8x5/8 in. self-tapping screws at 2-2/3 in. (6,8 cm) spacing. The models were placed upside down, and the extension of the columns were secured to the floor. The loading was applied with air pressure in rubberized canvas bags. The buckled shell in one of the tests is shown in Fig. 4.

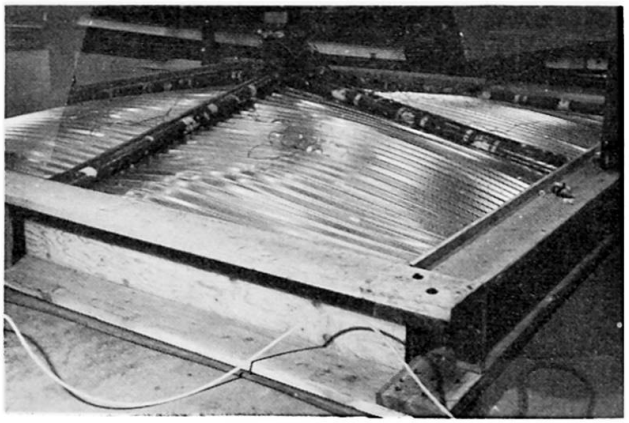

Fig. 4

Finite Element Analysis

The analysis of hypars is a highly complex subject. A number of approaches were based on shallow shell theories to evaluate bending effects and buckling. Often finite-difference solutions have been used. The difficulty with these approaches is the proper consideration of complex boundary conditions, especially in the case of thin-steel structures.

The finite element technique offers a method that can include a number of variables, such as orthotropy, edge member bending in two directions, the eccentricity of connection between the deck and the edge members, local loads, and various support conditions, in a systematic fashion. Two finite element solutions were developed by Banavalkar [3] as part of the present investigation: one used flat rectangular elements, the other employed curved shell elements rectangular in plan. The former is a special case of the latter.

The displacement fields for the curved elements were assumed to be linear for u and v, and the cross product of Hermitian polynomials for w. Linear strain-displacement relationships were utilized. The third strain component is

$$\gamma_{xy} = u_y + v_x - \frac{2c}{ab} w \qquad (1)$$

since the equation of the surface is

$$z = \frac{c}{ab} xy \tag{2}$$

The total strain energy is caused by membrane stresses, shell bending, and edge member bending, twisting, axial straining, and warping. The displacement fields for the edge members were linear for axial displacements, and nonlinear cubic for transverse and twist displacements. The possibility of relative displacements at the connection between the deck and the edge members was considered in the analysis.

In the instability analysis, the change of potential energy caused by membrane forces was accounted for. This resulted in the following form of the stiffness equation

$$\{P\} = \Big[[K] + [N]\Big]\{D\} = [K_{eff}]\{D\} \tag{3}$$

where [K] is the master stiffness matrix, [N] is the incremental stiffness matrix that is equal to the second derivative of the potential energy of the membrane forces, and {P} and {D} are the load and displacement vectors, respectively. The matrix [N] depends on the in-plane forces, and therefore also on the normal displacements.

In the present investigation a load incrementation method was used instead of a direct eigenvalue evaluation. The load-deflection curve exhibits a rapid change in slope at instability. In each load step the in-plane forces N_x, N_y, and N_{xy} were evaluated from {D} using a linear analysis. The new stiffness matrix $[K_{eff}]$ in Eq. (3) was used in subsequent iterations. This procedure was repeated at each load level. The analysis was verified by comparisons with Reissner's approach for the isotropic, fully supported case, and with other finite element studies.

Example

A hypar roof is composed of four units and is supported by four 10 in. (25,4 cm) square tubular columns (Fig. 5). It covers an area of 60 ft by 60 ft (18,3 m by 18,3 m). The low points A, B, C, D are connected with 3 in. (7,6 cm) diameter rods along the perimeter. The top horizontal edge members are W30X99 and the sloping outside members are W18X64. The deck is connected eccentrically to the horizontal edge members. The deck is made of two corrugated layers (Fig. 3) with thicknesses of h = 0.0747 in. (1,9 mm), and f = 0.375 in. (9,5

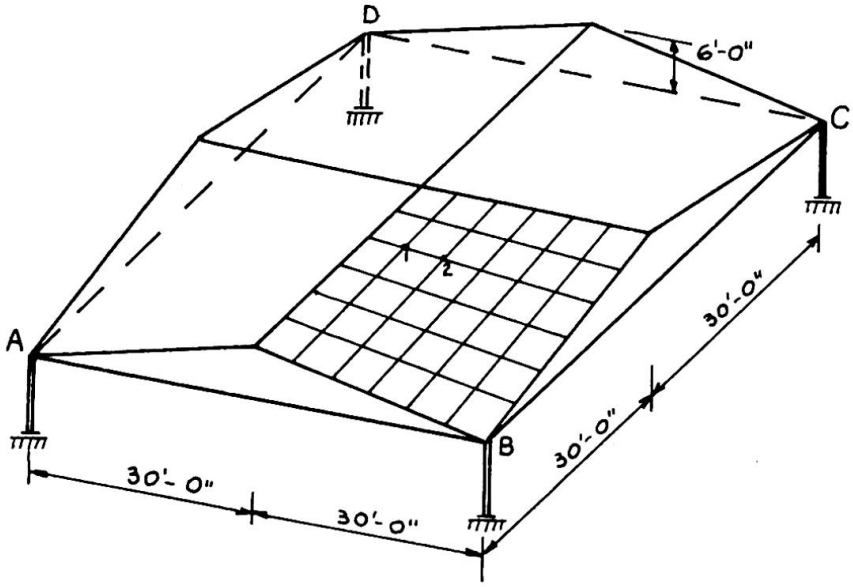

Fig. 5

mm), r = 1.5 in. (3,8 cm). The effective shear stiffness of the units was estimated from flat shear tests to be 0.10Gh.

Deck buckling analysis was carried out by specifying several load steps and three iterations at each load level. The deflections at two selected points (Fig. 5) are plotted in Fig. 6. It is seen that buckling occurs at a load of about 65 psf (320 kg/m^2).

The buckling analysis predicted about 60 psf (295 kg/m^2) critical load for the experiment of Fig. 4; the measured value was about 75 psf (370 kg/m^2). It is suspected that the actual shear rigidity was greater than the value assumed in the analysis.

Analyses indicate that prebuckling deflections and the bending stiffness of edge members have little effect on instability, but the axial stiffness of edge members does influence it somewhat. The deck buckling load of hypars with two layers is ordinarily at least three times greater than that of similar structures with single layers of decking.

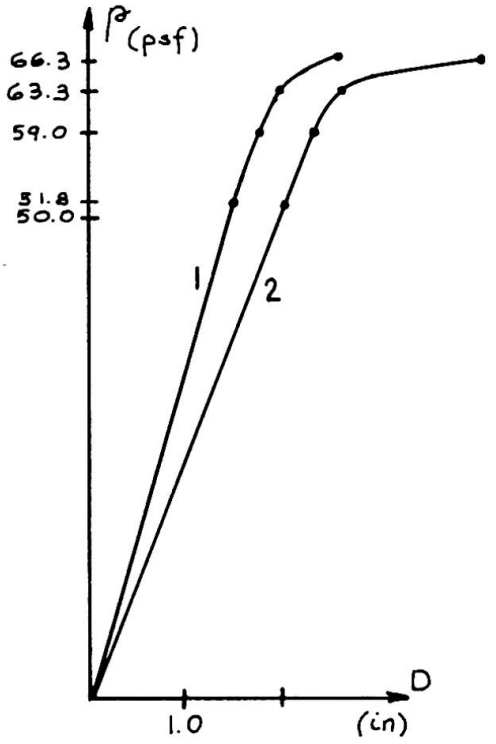

Fig. 6

Energy Analysis

The finite element instability analysis involves considerable computer expense. In order to aid in preliminary designs, an approximate deck buckling analysis was also developed.

The potential energy V of an orthotropic shell is [3, 5]

$$V = \frac{1}{2}\int_0^B\int_0^A [D_x w_{xx}^2 + 2D_1 w_{xx}w_{yy} + D_y w_{yy}^2 + 4D_{xy}w_{xy}^2 + 4G_{eff}h(c/ab)^2 w^2 + 2N_{xy}w_x w_y]dxdy \qquad (4)$$

where the subscripts denote partial derivatives and $N_{xy} = pab/2c$ is the membrane shear force in the shell under uniform loading p. The assumed deflected shape was

$$w = \sin\frac{\pi y}{b}\sin[\frac{n\pi}{a}(x - sy)] \qquad (5)$$

where s is the tangent of the angle of the buckles measured from the y axis, and n is the number of buckled waves. This displacement function gave good results in the buckling analysis of flat shear diaphragms.

The substitution of w into Eq. (4) yields

$$p_{cr} = \frac{c}{abs}\left(\frac{\pi}{b}\right)^2 [D_x\beta^2 + 2D_1(1+\beta^2 s^2) + D_y(1/\beta^2 + \beta^2 s^4 + 6s^2 + 4D_{xy}(1+\beta^2 s^2) + \bar{G}/\beta^2] \qquad (6)$$

where

$$\beta = \frac{nb}{a} \quad \text{and} \quad \bar{G} = \frac{4G_{eff}h}{\pi^4}\left(\frac{bc}{a}\right)^2$$

This expression has to be minimized with respect to s and n. The buckled shape for a hypar unit with single layer of corrugated sheet decking is shown in Fig. 7.

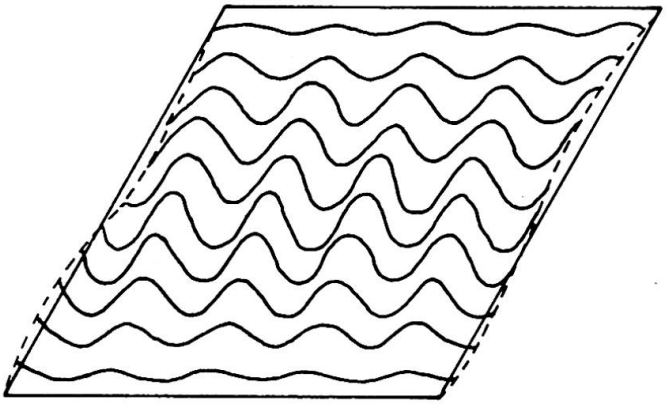

Fig. 7

Computer-aided analyses gave results that agreed well with finite element calculations and with tests. For the aforementioned example the buckling load from the energy analysis is 51 psf (250 kg/m²) that occurs at 44.4 degrees and with three half sine waves.

The computer time involved in the search of the minimum of p_{cr} is very small and therefore numerous analyses can be performed with little expense. Comparative studies to determine the relative importance of variables indicate that the buckling load of single corrugated shells is roughly proportional to

$$\frac{\sqrt[3]{\alpha}}{b^2}\left(\frac{hc}{a}\right)^{\frac{3}{2}} \qquad (7)$$

where α is a nondimensional shear rigidity factor $\alpha = G_{eff}/G$. The accuracy of the factor (7) is indicated in Fig. 8 for standard (f = 0.25 in. and r = 1.33 in.) and deep (f = 0.375 in. and r = 1.50 in.) corrugated decks. In the case of double layers, the factor (7) is approximately linear with h.

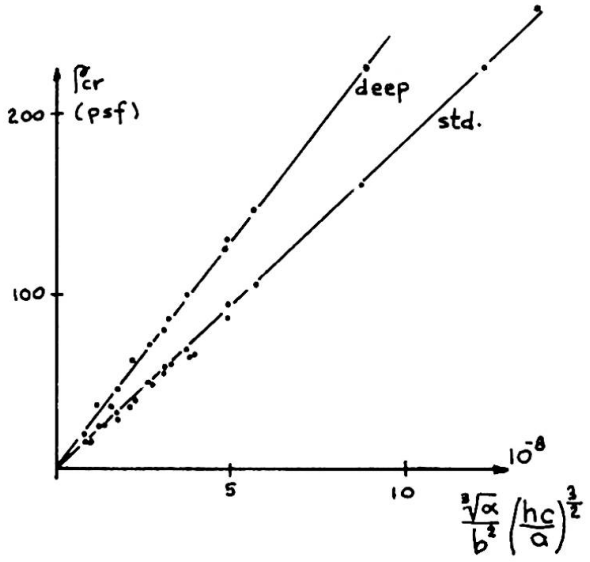

Fig. 8

For single layer shells the bending rigidity in the strong direction (D_y) is, by far, the most important rigidity factor, and p_{cr} varies approximately as $\sqrt{D_y}$. For corrugated decks D_y is approximately equal to

$$D_y \approx \frac{Ef^2h}{3}\left(1.6 + \frac{f}{2r}\right) \qquad (8)$$

The effect of D_x is much less, and the influence of D_{xy} and D_1 is negligible for corrugated shells, in fact, D_1 can be taken as zero. But, as mentioned previously, the most important variables affecting the behavior of thin-steel hypars are the curvature c/ab and the effective shear rigidity.

The approximate buckling analysis and the simple membrane theory may be sufficient in the design of minor structures, such as roofs for service stations. However, in the final design of major structures more complex analyses, for example using the finite element method, must be used to calculate buckling loads, deflections, and stresses.

Acknowledgments

The investigation of thin-steel hypars at Cornell University was supported by the American Iron and Steel Institute. The project was under the general direction of Dr. George Winter. The contribution of Messrs. P. V. Banavalkar, J. E. Parker, A. Banerjee, and R. Muskat is gratefully acknowledged.

References

1. Gergely, P., and Parker, J. E., "Thin-Walled Steel Hyperbolic Paraboloid Structures," Eighth Congress, IABSE, Final Report, New York, 1968.
2. Luttrell, L. D., "Strength and Behavior of Light Gage Steel Shear Diaphragms," Cornell Engineering Research Bulletin, No. 67-1, Department of Structural Engineering, Cornell University, 1967.
3. Gergely, P., Banavalkar, P. V., and Parker, J. E., "The Analysis and Behavior of Thin-Steel Hyperbolic Paraboloid Shells," Report No. 338, Department of Structural Engineering, Cornell University, September 1971.
4. Reissner, E., "Some Aspects of the Theory of Thin Elastic Shells," Journal, Boston Society of Civil Engineers, Vol. XLII, No. 2, April 1956.
5. Gergely, P., "Buckling of Orthotropic Hyperbolic Paraboloid Shells," Proc. Journal of the Structural Division, American Society of Civil Engineers, Vol. 98, No. ST1, January 1972.

Summary

The design of hypar shell roofs with thin-steel decking is often controlled by deflections and buckling. Finite element and approximate energy instability analyses are described that may be used by designers. Experiments confirmed the analytical approaches.

Leere Seite
Blank page
Page vide

Weitgespannte Sandwichkuppel im Werkstoffverbundsystem Stahlfeinblech-Polyurethanschaum

Large Span Sandwich Dome in Composite Material System of Thin Steel Plate and Polyurethan Solid Foam

Coupole de grande portée en construction sandwich tôle d'acier – mousse de polyuréthane

OTTO JUNGBLUTH
Professor Dr.-Ing.
Bochum, BRD

1. Leichte Flächentragwerke

Bei Flächentragwerken des konstruktiven Ingenieurbaus wird das Verhältnis Konstruktions-Eigengewicht zur Gesamtbelastung mit wachsender Spannweite immer ungünstiger. Um den Nachteil des hohen Konstruktionseigengewichtes bei weitgespannten Flächentragwerken zu vermeiden, verfolgt man neuerdings zwei Wege:

1. Auflösung des Flächentragwerks in zugbeanspruchte Seil- und Seilnetztragwerke
2. Flächentragwerke aus leichten Werkstoffen, z. B. verstärkten Kunststoffen.

Der erste Weg hat den Nachteil, daß das Seilwerk - weil im engeren Sinn eigentlich kein Flächentragwerk - doch zusätzlich mit kleineren Flächenträgern eingedeckt werden muß, und daß der konstruktive Aufwand des Verbundes zwischen Seilwerk und Dachhaut hohe Kosten verursacht.

Der zweite Weg der ausschließlichen Verwendung von Kunststoffen läßt trotz der möglichen Verstärkung mit Fasereinlagen wegen der ungünstig wirkenden Langzeitbeanspruchung keine großen Spannweiten zu. Außerdem ist das zusätzliche Aufbringen von Dämmschichten schwierig und wirtschaftlich kaum vertretbar.

Deshalb verfolgt der Verfasser seit über 10 Jahren einen dritten Weg, nämlich das Ausnützen des günstigen Festigkeits-Gewichts-Verhältnisses von Stahlfeinblechdeckschichten und deren Stabilisierung durch eine gleichzeitig als Wärmedämmung wirkende Kunststoff-Kernschicht. [1]

Über das günstige Tragverhalten von Sandwichflächentragwerken des Werkstoff-Verbundsystems Stahlfeinblech-Polyurethanhartschaum und über die Planung einer 45 m weit gespannten Sandwichkuppel wurde bereits während des VIII. Kongresses in New York 1968 berichtet. [2]

Inzwischen wurde diese Kuppel ausgeführt und im Jahre 1970 der Fachwelt vorgestellt.

2. Werkstoffverbundsystem Stahl/Polyurethan

Der Grund, daß Stahlbleche trotz ihrer hohen Festigkeit bisher nur in wenigen Fällen - eigentlich nur in zwei - als Flächentragwerke eingesetzt wurden, nämlich als Tankdächer im Behälterbau und als Stahlfahrbahn im Großbrückenbau, liegt in der aufwendigen Aussteifung gegen Instabilitäten. So beträgt der Gewichtsauf-

wand für Steifen im Verhältnis zum Blech

im Brückenbau ca. 25 - 30 %
im Behälterbau ca. 30 - 40 %

Der Ersatz der diskontinuierlichen Steifen durch die kontinuierliche Bettung des Bleches mit Hilfe der Dämmschicht und die Verwendung des selbstklebenden, selbstreagierenden Polyurethan-Gemisches als Hartschaum-Stützschicht sind als der entscheidende Durchbruch zu einer wirtschaftlichen Sandwich-Flächentragwerk technik im Hochbau anzusehen. [3]

Die erfolgreiche und sichere Anwendung des Sandwichsystems Stahl/Polyuretha (FEPUR) ist aber an eine entscheidende Bedingung, die nicht unbedingt eine Einschränkung bedeuten muß, gebunden. Auch Polyurethanhartschaum ist als Kunststoff eine organische Substanz, die bei entsprechend hoher Langzeitbeanspruchung zum Kriechen neigt. Es ist deshalb wichtig, zwei Wirkungen der Sandwichkernschicht zu unterscheiden:

1. für ebene Sandwichflächentragwerke vorzugsweise eine Schubübertragung zwischen den beiden Deckschichten,
2. für profilierte und gewölbte Sandwichflächentragwerke vorwiegend eine Stabilisierung der beiden Deckschichten.

Wie auch Versuche inzwischen bestätigt haben, ist die abträgliche Kriechneigung des Polyurethan-Hartschaums bei Langzeitbeanspruchung nur im ersten Fall zu beobachten. Deshalb kommen ebene FEPUR-Sandwichflächentragwerke nur für gering beanspruchte Wandelemente, z. B. für Hallenbeplankungen, in Frage. Für höher beanspruchte Dachtragwerke kann die Kriechneigung des Kunststoffschaums durch eine Konstruktionsform nach Fall 2 ausgeschlossen werden.

Um die Vermeidung der Kriechwirkung bei profilierten und gewölbten Sandwich Flächentragwerken im praktischen Langzeit-Großversuch zu beweisen, wurde die Sandwichkuppel Hannover nach Vorschlag des Verfassers von den Firmen Hoesch (Stahl) und Bayer (Polyurethan) errichtet.

Als Werkstoffe wurden verwendet:

Stahlfeinblech der Güte St 37 mit einer Streckgrenze σ_s = 24 kp/mm^2, 25 μ feuerverzinkt und kunststoffbeschichtet

Polyurethan mit den Komponenten des Schäumgemisches:

a)	Polyol FWFA (Bayer)	100 Gew. teile
b)	Polyol TM (Bayer)	1 " "
c)	Isocyanat 44 V (Bayer)	105 " "
d)	Aktivator Desmorapid PP (Bayer)	2 " "
e)	Treibmittel R 11 (Kali-Chemie) Fluortrichlormethan	30 " "

Sowohl aus freigeschäumtem Material als auch aus Versuchs-Sandwichelemente wurden Probekörper entnommen, deren Prüfung folgende Werkstoffkennwerte ergal

Raumgewicht	78 kg/m^3	Würfel 10/10/10 cm
"	81 "	" 5/ 5/ 5 cm
Druckstabilität	5,1 "	" 5/ 5/ 5 cm
Zerreißfestigkeit	5,5 "	" 10/10/10 cm

Konturänderung bei 80°C 3 Stunden	0,0 %	Würfel 10/10/10 cm
Konturänderung bei -20°C 3 Stunden	0,0 %	" 10/10/10 cm

Die Haftfestigkeit des PU-Schaums am Stahlblech muß so groß sein, daß bei Zerreißversuchen an Probekörpern der Bruch im Schaumkern und nicht in der Haftfuge erfolgt.

3. Konstruktion

Das Kuppeltragwerk hat die in Bild 1 dargestellten Abmessungen. Die Kugel-

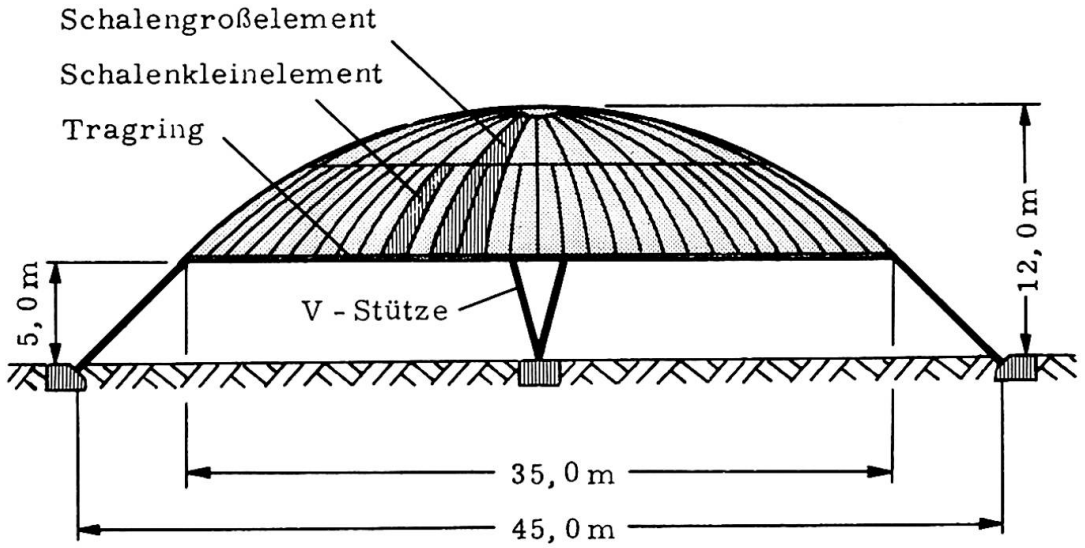

Bild 1

schale mit einem Krümmungsradius R = 24,7 m in Meridianrichtung besteht aus 40 Großsegmenten von je 18,69 m Länge und einer Basisbreite von 2,74 m am Fußring (Bild 2). Aus fertigungstechnischen Gründen sind die Großsegmente nur einfach, und zwar in Meridianrichtung gekrümmt.

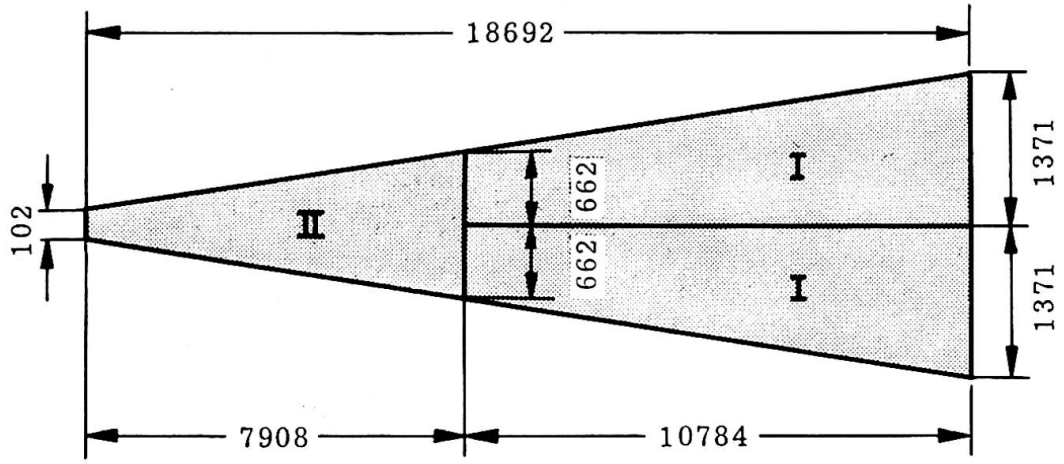

Maße in mm

Bild 2

Die Gesamtdicke des Sandwich-Querschnitts beträgt 150 mm (Bild 3), die Stahldeckschichten sind je 1 mm dick und wurden nur an den Lasteinleitungsstellen der

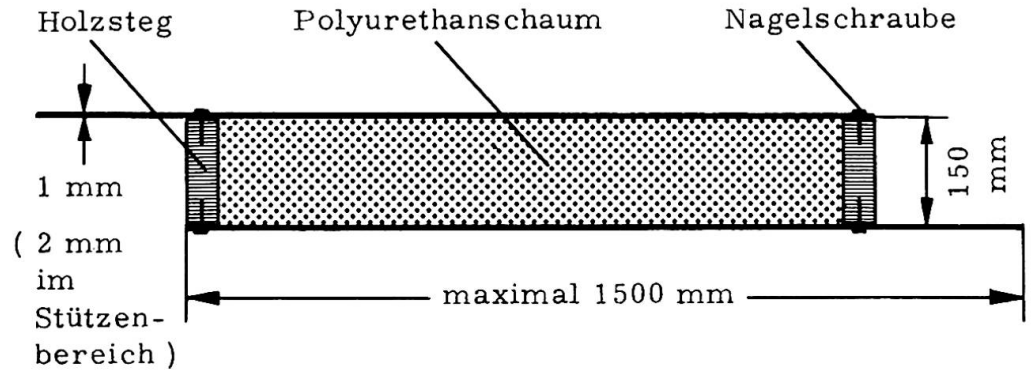

Bild 3

Stützen auf 2 mm verstärkt. Da Stahlfeinblech in der gewählten Segment-Basisbreite nicht hergestellt wird, und da das Ausschäumen so großer Elemente in einer fast 19 m langen Form zu schwierig geworden wäre, wurde das Segment für die Herstellung nochmals in drei Schalenkleinelemente (Bild 2) unterteilt. Die seitlichen Längsränder wurden durch Holzstege abgeschottet, wobei der eine Längsrand jedes Deckblechs zur Schaffung einer Überlappverbindung um je 145 mm überstand. Die Verbindung der Stahlbleche mit den Holzstegen erfolgte mit Nagelschrauben, die Überlappverbindung von Deckblech zu Deckblech mit Blindnieten 4,8 mm ϕ. Der Abstand der Nagelschrauben variiert zwischen 70 mm im unteren und 180 mm im oberen Bereich der Kuppel.

Der Fußring, der die 40 Sandwichgroßsegmente an der Basis aufzunehmen hat, ist ein regelmäßiges Vierzigeck mit Kastenquerschnitt (Bild 4). Die vier V-Stützen sind ebenfalls Kastenprofile.

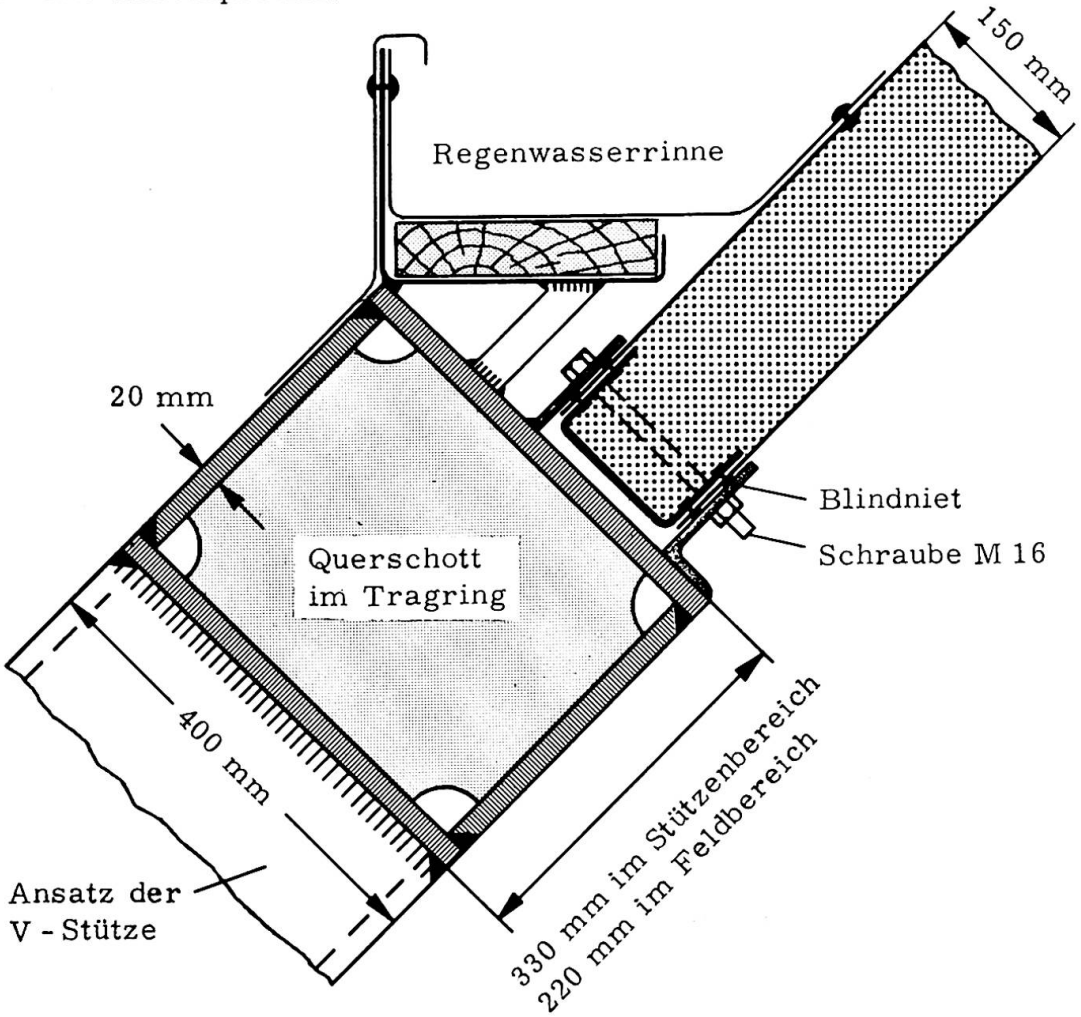

Ein Schalengroßsegment wiegt einschließlich der Verbindungsfugen 1045 kp, also rund 1 to. Die Leistungsfähigkeit des Werkstoffverbundsystems Stahl/Polyurethan wird am besten aus dem folgenden Vergleich von Kuppeln etwa gleicher Spannweite, aber aus verschiedenen Baustoffen und nach verschiedenen Bauweisen deutlich:

	Eigengewicht
Kuppel Petersdon Rom	$g = 2600\ kp/m^2$
Stahlbetonkuppel	$g = ca.\ 200\ kp/m^2$
Sandwichkuppel Hannover	$g = 30\ kp/m^2$

Hierbei ist noch zu beachten, daß in diesem geringen Gewicht des Sandwichtragwerks noch das Eigengewicht der Wärmedämmung des von keinem anderen Dämmwerkstoff übertroffenen Polyurethans ($\lambda = 0,002$ kcal/m h C°) enthalten ist und der Witterungsschutz durch die Kunststoffbeschichtung des Stahlblechs.

Neben der hervorragenden Tragwirkung schließt das Sandwichsystem Stahl/Polyurethan (FEPUR) also noch die notwendigen bauphysikalischen Eigenschaften Wärmedämmung, Witterungsschutz und Dampfsperre sozusagen systemimmanent ein.

4. Berechnung

Der Berechnung lagen folgende Lastannahmen zu Grunde:

a) Eigengewicht

2 Stahlbleche à 1 mm:	$g = 2 \cdot 7,85 =$	$15,7\ kp/m^2$
15 cm Polyurethanschaum: ($\gamma = 80\ kp/m^3$)	$g = 80 \cdot 0,15 =$	$12,0\ kp/m^2$
Holz-Randstege	$g =$	$\sim 3\ kp/m^2$
	$g \approx$	$30\ kp/m^2$

b) Schnee

Vollast	$p_s = 70\ kp/m^2$
halbseitige Last	$p_s = 50\ kp/m^2$

c) Wind

Symmetrischer Sog	$p_w = -95\ kp/m^2$
Antimetrischer Windanteil	$p_w = +50\ kp/m^2$

Die Druck- und Sogverteilung der Windlasten wurde auf Grund von Windkanalversuchen am offenen und geschlossenen Modell ermittelt.

Die Standsicherheitsnachweise hatten folgendes Ergebnis:

4.1 Spannungsnachweis:

Die größte Spannung in den Stahldeckblechen der Sandwichschale im Bereich des Fußrings betrug:

$$\sigma_{max} = \pm 509\ kp/cm^2$$

4.2 Stabilitätsnachweis Knittern der Deckschichten:

Nach [1] und [5] gilt:

$$\sigma_{Ki} = 0{,}8 \cdot \sqrt[3]{E^D E^K G^K}$$

$$= 0{,}8 \cdot \sqrt[3]{2{,}1\ 10^6\ 70\ 30}$$

$$= 1300\ \text{kp/cm}^2$$

Fordert man eine zweifache Sicherheit, so ist eine Spannung von $\sigma = 650\ \text{kp/cm}^2$ für die Deckbleche zulässig. Im vorliegenden Fall wirkt sich außerdem noch die Zugspannung des zweiachsigen Spannungszustandes günstig, d.h. stabilisierend aus.

4.3 Nachweis der Gesamtstabilität

Bei der stark gewölbten Kuppel war ein Durchschlagen nicht zu erwarten, das ergaben auch die beiden Nachweise

a) nach [4]

$$p_D = c \cdot E \left(\frac{\delta}{R}\right)^2 = 3{,}77\ M_p/m^2$$

mit $p_{vorh} = 0{,}108$ wird

$$\nu_D = \frac{3{,}77}{0{,}108} = 35$$

b) nach [5] für weiche Kerne:

$$\nu_D = \frac{2\,S}{R} = \frac{2 \cdot 30 \cdot 1500}{24{,}70} = 4{,}05$$

$$\nu_D = \frac{4{,}05}{0{,}108} \quad 40$$

5. Fertigung und Montage

Für die Fertigung der Sandwich-Schalenkleinelemente wurden zur abwechselnden Betriebsweise zwei gleiche Schäumvorrichtungen (Bild 5) gebaut, die so ausgelegt waren, daß sie den auftretenden Schäumdruck von etwa $p = 2\ \text{kp/cm}^2$ aufnehmen konnten. Die zugeschnittenen verzinkten und kunststoffbeschichteten Stahlfeinbleche wurden in die Schäumform eingelegt und an den Rändern mit den Holzstegen durch die Nagelschrauben verbunden, so daß nach Schließen der Deckelteile der Schäumform ein allseits geschlossener Hohlraum entstand, in den bei den oberen Schalenkleinelementen (Typ I) durch ein und bei den unteren (Typ II) durch zwei Einfüll-Löcher das Polyurethankomponentengemisch eingespritzt werden konnte. Die Schäummaschine HK 1000 hat eine maximale Austrittsleistung von 190 kg/min. Für das größere untere Schalenkleinelement (Typ II) mit einem Schaumkernvolumen von $1{,}46\ m^3$ betrug bei einer Austrittsleistung von 2,6 kg/sec die eingeschossene Menge 120 kg bei einer Einschußzeit von 46 Sekunden. Für das kleinere Firstschalenelement mit $0{,}72\ m^3$ Volumen wurde die erforderliche Menge des Polyurethangemisches von 60 kg in 23 Sekunden eingespritzt. Bei dem im Hinblick auf eine gleich-

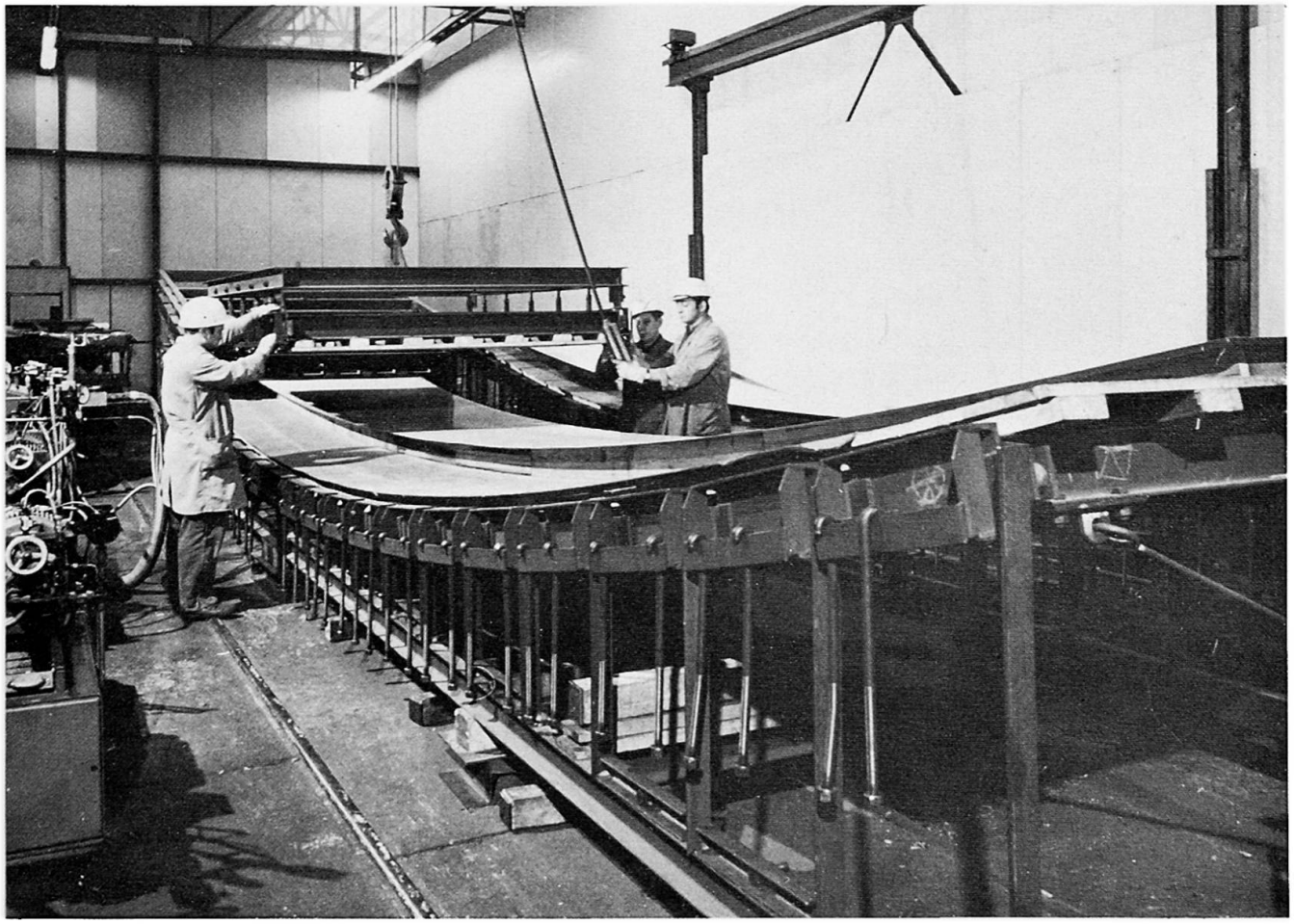

Bild 5

mäßige Schaumstruktur gewählten Verdichtungsgrad von 1:2, d.h. dem Verhältnis von freiverschäumtem zu formverschäumtem Raumgewicht, baute sich ein Schäumdruck von ca. 2 kp/cm^2 auf. Die Aushärtezeit betrug in Anbetracht des großen Schaumvolumens und im Hinblick auf die noch geringen Erfahrungen bei der erstmalig in dieser Größe für "tragende Bauteile" angewandten FEPUR-Sandwichtechnik 3-5 Stunden. Auf Grund der gewonnenen Erfahrungen kann aber angenommen werden, daß bei so großen FEPUR-Sandwichelementen die Ausschalzeit auf 1-2 Stunden gesenkt werden kann. Die in einer Versuchswerkstätte der Hoesch AG in Dortmund hergestellten Schalenkleinelemente wurden auf Tiefladern zur Baustelle der Messe Hannover gebracht, wo jeweils drei (Bild 2) in einer Halle zu einem Großsegment zusammengebaut wurden.

Zur Montage wurde zunächst ein Stahlrohr-Lehrgerüst errichtet und darauf die acht Teilstücke des Fußrings montiert und verschweißt, so daß anschließend die vier V-Stützen mit dem Fußring verschweißt werden konnten.

Die vierzig vormontierten Sandwich-Großsegmente von etwa 19 m Länge, 3 m Fußbreite und ca. 1 to Gewicht wurden mit einem Autokran auf den Fußring und das Lehrgerüst aufgelegt (Bild 6). Nach dem Ausrichten wurden die überlappenden Deckbleche mit Blindnieten und die Sandwich-Großelemente mit dem Fußring durch 5 Schrauben M 16 verbunden (Bild 7).

Die Meridianfugen der Großsegmente, die auch die Toleranzen aufzunehmen hatten und auf Grund der Kugelgeometrie zwischen 20 mm am oberen Ende - 85 mm in halber Höhe - und 20 mm am unteren Ende variieren, wurden anschließend mit einer kleineren Baustellenschäummaschine ausgeschäumt. Obwohl das Fugenschäu-

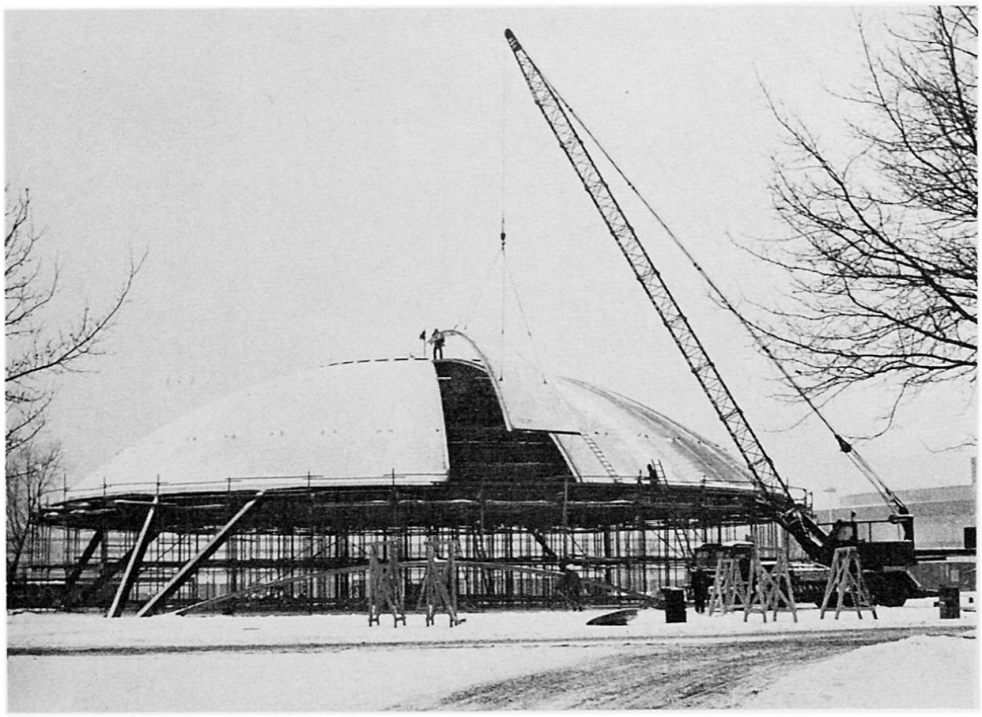

Bild 6

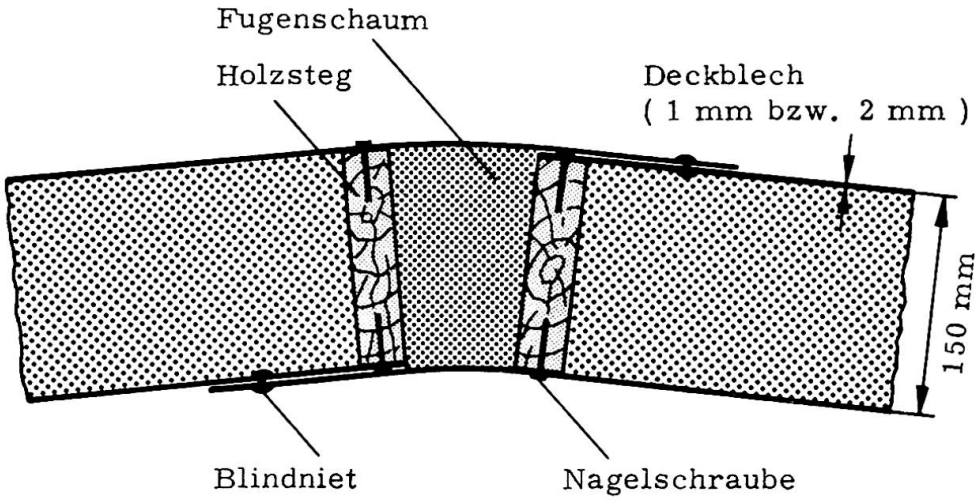

Bild 7

men im Winter durchgeführt wurde, konnte von der zunächst vorsichtshalber vorgesehenen Erwärmung der Fugen durch elektrische Heizmatten abgesehen werden, da sich zeigte, daß auch ohne diese Maßnahmen ein einwandfreier Haftverbund erreicht wurde.

Nach dem Ausschäumen der Fugen wurden Kuppel und Fußring vom Lehrgerüst freigesetzt (Bild 8).

Bild 8

6. Ausblick

Daß diese wohl erstmalig für eine "tragende Konstruktion" und noch dazu mit einer so großen Spannweite von 45 m errichtete Sandwichkugelschale aus 1 mm dickem Stahlblech und 150 mm dickem Polyurethan-Schaumkern eine sehr große Steifigkeit erzielte, zeigte sich bereits nach dem Freisetzen vom Montagegerüst, als eine Mittendurchsenkung von nur 5 mm gemessen wurde.

Aber würde diese Steifigkeit auch langfristig erhalten bleiben oder würden sich das Langzeitverhalten nachteilig beeinflussende Deformationen infolge Kriechen des Schaumkerns ergeben?

Seit der Nullmessung auf dem starren Gerüst am 10. 2. 1970 wurden bisher über einen Zeitraum von etwa 1 1/2 Jahren 20 über die Sandwichkugelschale verteilte Zielpunkte geodätisch vermessen. Die Verformungen der einzelnen zwanzig verteilten Meßpunkte liegen im Bereich weniger Millimeter oder Zehntelmillimeter. Unter ihnen haben einige der Meßpunkte infolge der Temperaturänderung der Jahreszeiten positive und negative Vorzeichen.

Ohne Berücksichtigung des Temperatureinflusses betrug die Höhenverschiebung des Kugelpols

	Durchsenkung	Differenz
10. 2. 70 (Nullmessung auf starrer Lagerung)	0	
		- 4,8
13. 2. 70	- 4,8	
		- 1,2
27. 2. 70	- 6,0	
		- 1,4
14. 5. 70	- 7,4	
		+ 2,3
26. 5. 71	- 5,1	

Dieses günstige Langzeitverhalten läßt erwarten, daß das neuartige Werkstoffverbundsystem Stahl/Polyurethan (FEPUR) im Konstruktionssystem der Sandwichtechnik zur Grundlage einer neuen Tragwerkstechnologie des konstruktiven Ingenieur-

baus werden wird. Voraussetzung ist allerdings, daß die Konstruktionsformen in Anpassung an dieses Werkstoffverbundsystem gestaltet werden.

Über bereits in der Entwicklung befindliche FEPUR-Sandwichbauteile für ein Fertigteilsystem und deren kontinuierlich-verfahrenstechnische Herstellung auf einer automatisierten Fertigungslinie wird zu gegebener Zeit berichtet.

Literaturhinweise

1 O. Jungbluth/H. Witte

"Das Verbundsystem Stahl/Kunststoff in der Sandwichtechnik"
HOESCH-Berichte aus Forschung und Entwicklung 3/68

2 O. Jungbluth

"Sandwichflächentragwerke im Stahlbau"
IVBH VIII. Kongreß New York, Schlußbericht Seite 333 - 343

3 O. Jungbluth

"Sandwichflächentragwerke im konstruktiven Ingenieurbau"
Rheinisch-Westfälische Akademie der Wissenschaften, Düsseldorf, Vortrag N 208

4 K. Klöppel/O. Jungbluth

"Beitrag zum Durchschlagproblem dünnwandiger Kugelschalen. (Versuche und Bemessungsformeln"
DER STAHLBAU 1953, Seite 121-130

5 F.J. Plantema

"Sandwich Construction"
John Wiley Inc. New York, London, Sidney 1966

Zusammenfassung

Es wird die Konstruktion, Herstellung und Montage einer 45 m weitgespannten Sandwichkugelschale aus dem Werkstoff-Verbundsystem Stahl/Polyurethan beschrieben.
Das bisher über eineinhalb Jahre verfolgte günstige Langzeitverhalten der Sandwichkuppel läßt erwarten, daß dieser Werkstoffverbund von Stahl und Kunststoff in der Konstruktionsform der Sandwichtechnik eine neue leistungsfähige und wirtschaftliche Leichtbau-Tragwerkstechnologie begründet.

Cylindrical Shells Made of Corrugated Sheets

Coques cylindriques en tôles nervurées

Zylinderschalen aus gerippten Blechen

G. ABDEL-SAYED
Associate Professor

M.N. EL-ATROUZY
Research Assistant

Department of Civil Engineering
University of Windsor
Windsor, Ontario, Canada

INTRODUCTION

The advantages of using light gauge steel sheets in folded plate roofs has been established through studies and practical applications in both Canada and the U.S.A. It is also generally recognized that cylindrical shell roofs have better carrying characteristics, as they translate the applied loads into mainly membrane forces. Furthermore, corrugated sheets with cylindrical curvature are widely available and so far they are employed mainly in non-structural capacities.

This study is to establish methods of analysis and also economical applications of cylindrical shells made of corrugated sheets.

GOVERNING DIFFERENTIAL EQUATIONS

The shells are considered as being made of elastic orthotropic material in which the mechanical properties are equal to the average properties of the corrugated sheets. For the arc-and tangent-type of corrugation, Fig. 1, these properties are [1,3]:

$$D_\phi = \frac{\ell}{c}\, t\, E \qquad (1a)$$

$$D_x = \frac{E}{6(1-\mu^2)} \left(\frac{t}{f}\right)^2 t \qquad (1b)$$

$$D_{x\phi} = \rho \frac{Et}{2(1+\mu)} \frac{c}{\ell} \qquad (1c)$$

$$B_\phi = 0.522\, Ef^2 t \qquad (1d)$$

$$B_x = \frac{c}{\ell} \frac{Et^3}{12(1-\mu^2)} \qquad (1e)$$

$$B_{x\phi} = \frac{\ell}{c} \frac{Et^3}{12(1+\mu)} \qquad (1f)$$

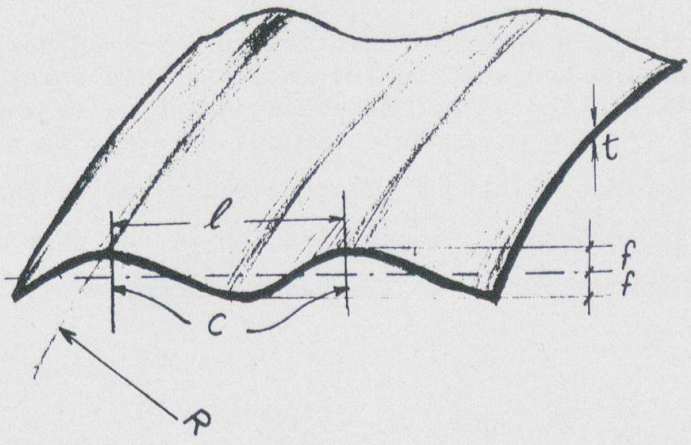

Fig. 1: Arc-and Tangent Corrugation

in which: D_x and D_ϕ = axial ridigity in the x- and ϕ directions respectively; $D_{x\phi}$ = shear rigidity in the $x\phi$-plane; B_x and B_ϕ = bending rigidity in the xz- and ϕz-planes respectively; $B_{x\phi}$ = torsional rigidity; t = average thickness of the sheet;

c = corrugation pitch; ℓ = developed length of corrugation per pitch; f = half depth of corrugation; E = modulus of elasticity of steel; μ = Poisson's ratio; and ρ = a reduction factor to account for the effect of slip at sheet to sheet and sheet to frame connections [3].

The differential equations governing the behaviour of the shell are obtained by using the above mentioned properties together with the equilibrium conditions and geometric relationships of an infinitismal element dx.Rdϕ. These equations are:

$$D_x \ddot{u} + \frac{B_x}{R} \dddot{w} + D_{x\phi}\left(\frac{\ddot{u}}{R^2} + \frac{\dot{v}'}{R}\right) + \frac{B_{x\phi}}{2R^3}\left(\frac{\ddot{u}}{R} - \dot{w}''\right) + p_x = 0 \qquad (2a)$$

$$D_\phi(\ddot{v} - \dot{w}) + D_{x\phi}(R\dot{u}' + R^2 v'') + \frac{3B_{x\phi}}{2}(v'' + \dot{w}'') + p_\phi R^2 = 0 \qquad (2b)$$

$$D_\phi(\dot{v} - w) - \frac{B_y}{R^2}(w'''' + 2w'' + w) - (B_x R^2 w'''' + B_x R u''') - (2B_{x\phi}\dddot{w} + B_{x\phi}\dot{v}''$$

$$- \frac{B_{x\phi}}{2R}\ddot{u}' + \frac{B_{x\phi}}{2}\dot{v}'') + p_z R^2 = 0 \qquad (2c)$$

in which $\dot{(\ )} = \frac{\partial(\ )}{\partial\phi}$, $(\ )' = \frac{\partial(\ )}{\partial x}$; p_x, p_ϕ and p_z are the components of the surface (external) loading in the x-, ϕ- and z- directions respectively.

The system of equations, Eqs. 2a, b, c, is derived without approximation. It encounters a number of terms which have insignificant effect on the results in shallow and/or short shells. These terms may be neglected and the system of equations is simplified as follows:

$$D_x u'' + D_{x\phi}\left(\frac{\ddot{u}}{R^2} + \frac{\dot{v}'}{R}\right) + p_x = 0 \qquad (3a)$$

$$D_\phi(\ddot{v} - \dot{w}) + D_{x\phi}(R\dot{u}' + R^2 v'') + p_\phi R^2 = 0 \qquad (3b)$$

$$D_\phi(\dot{v} - w) - (B_x R^2 w'''' + 2B_{x\phi}\dddot{w} + \frac{B_\phi}{R^2}\ddot{w}'') + p_z R^2 = 0 \qquad (3c)$$

METHOD OF SOLUTION

First, a membrane solution is obtained for the governing differential equations considering the surface loading. In this solution the boundary conditions are not satisfied. Thereafter a bending solution of the equations with no surface loading, $p_x = p_\phi = p_z = 0$, is superimposed in order to satisfy the boundary conditions.

A - Membrane Solution: The external load is analysed in its three components p_x, p_ϕ and p_z. As an example, a snow loading in the form of a sine wave, with maximum intensity p at the crown of the shell, has the components:

$$p_x = 0 \qquad (4a)$$

$$p_\phi = \frac{-4p}{n\pi}\cos(\phi_e - \phi)\sin(\phi_e - \phi)\cos\frac{\lambda x}{R} \qquad (4b)$$

$$p_z = \frac{4p}{n\pi}\cos^2(\phi_e - \phi)\cos\frac{\lambda x}{R} \qquad (4c)$$

in which $\lambda = \frac{\pi R}{L}$; L and R = the length and radius of curvature of the shell respectively; ϕ_e = half the central angle.

The membrane solution corresponding to the given snow loading is:

$$N_x = -\frac{12p}{R\pi k^2}\cos 2(\phi_e-\phi)\cos kx \tag{5a}$$

$$N_\phi = -\frac{4pR}{\pi}\cos^2(\phi_e-\phi)\cos kx \tag{5b}$$

$$N_{x\phi} = \frac{6pL}{\pi^2}\sin 2(\phi_e-\phi)\sin kx \tag{5c}$$

$$w = \frac{12p}{\pi}\left[\frac{1}{D_{x\phi}k^2}+\frac{4}{R^2k^4D_x}\right]\cos 2(\phi_e-\phi)\cos kx \tag{5d}$$

$$v = -\frac{6p}{\pi}\left[\frac{1}{D_{x\phi}k^2}+\frac{4}{R^2k^4D_x}\right]\sin 2(\phi_e-\phi)\cos kx \tag{5e}$$

$$u = -\frac{12p}{Rk^3\pi D_x}\cos 2(\phi_e-\phi)\sin kx \tag{5f}$$

in which $k = \frac{\pi}{L}$.

B - Bending Solution: The bending solution can be assumed as follows:

$$w = E^* e^{m\phi}\cos\frac{\lambda x}{R},\quad u = F^* e^{m\phi}\sin\frac{\lambda x}{R},\quad v = G^* e^{m\phi}\cos\frac{\lambda x}{R} \tag{6a,b,c}$$

in which E^*, F^* and G^* are constants.

Eqs. 6a, b, c are substituted in the governing equations, Eqs. 2a, b, c, after replacing p_x, p_ϕ and p_z by zero. A non-trivial solution of the resulting homogeneous system of equations is governed by the following characteristic equation:

$$m^8 + m^6\left[2-\lambda^2\left(\frac{D_x}{D_{x\phi}}+\frac{2B_{x\phi}}{B_\phi}\right)\right] + m^4\left[\lambda^4\left(\frac{D_x}{D_\phi}+\frac{2D_xB_{x\phi}}{B_\phi D_{x\phi}}+\frac{B_x}{B_\phi}\right) - \lambda^2\left(\frac{2D_x}{D_{x\phi}}+\frac{2D_\phi B_x}{D_{x\phi}B_\phi}\right)+1\right]$$
$$+ m^2\left[-\lambda^6\left(\frac{D_xB_x}{D_{x\phi}B_\phi}+\frac{2D_xB_{x\phi}}{D_\phi B_\phi}\right) + \lambda^4\left(\frac{2D_x}{D_\phi}-\frac{2B_x}{B_\phi}+\frac{3D_xB_{x\phi}}{D_{x\phi}B_\phi}\right) - \lambda^2\left(\frac{2B_{x\phi}}{B_\phi}+\frac{D_x}{D_{x\phi}}\right)\right]$$
$$+ \left[\lambda^8\left(\frac{D_xB_x}{D_\phi B_\phi}\right) + \lambda^4\left(\frac{D_xR^2}{B_\phi}+\frac{3D_xB_{x\phi}}{2D_{x\phi}B_\phi}+\frac{D_x}{D_\phi}\right)\right] = 0 \tag{7}$$

A simplified characteristic equation can be obtained in a similar way by substituting Eqs. 6a, b, c in the simplified set of equations Eqs. 3a, b, c:

$$m^8 + m^6\left[-\lambda^2\left(\frac{D_x}{D_{x\phi}}+\frac{2B_{x\phi}}{B_\phi}\right)\right] + m^4\left[\lambda^4\left(\frac{D_x}{D_\phi}+\frac{2B_{x\phi}D_x}{B_\phi D_{x\phi}}+\frac{B_x}{B_\phi}\right)\right]$$
$$+ m^2\left[-\lambda^6\left(\frac{2B_{x\phi}D_x}{B_\phi D_\phi}+\frac{B_xD_x}{B_\phi D_{x\phi}}\right)\right] + \left[\lambda^8\left(\frac{D_xB_x}{D_\phi B_\phi}\right)+\lambda^4\left(\frac{D_xR^2}{B_\phi}\right)\right] = 0 \tag{8}$$

If isotropic properties are considered for the shell, Eq. 7 and Eq. 8 yield the well known characteristic equations of Flügge and Donnell respectively.

The roots of either Eq. 7 or Eq. 8 can be written as follows:

$$m = \pm\alpha_1 \pm i\beta_1 \quad\text{and}\quad m = \pm\alpha_2 \pm i\beta_2 \tag{9}$$

and the deflection, w:

$$w = \{e^{\alpha_1\phi}[A_n \cos\beta_1\phi + B_n \sin\beta_1\phi] + e^{-\alpha_1\phi}[C_n \cos\beta_1\phi + D_n \sin\beta_1\phi]$$

$$+ e^{\alpha_2\phi}[E_n \cos\beta_2\phi + F_n \sin\beta_2\phi] + e^{-\alpha_2\phi}[G_n \cos\beta_2\phi + H_n \sin\beta_2\phi]\} \cos\frac{\pi}{L}x \qquad (10)$$

The values of a set of roots, Eq. 9, are considered to be exact when calculated from Eq. 7 and approximate when calculated from the simplified Eq. 8. The deviations between these sets of roots increase with the increase of the ratios L/R. The average error in the 8-roots is taken as a base to determine the ratio L/R within which the simplified system of equations can be used with a reasonable degree of accuracy in the final results. Fig. 2 shows the percentage of the error versus L/R. It also shows a similar curve for the percentage of errors in the 8-roots when using the simplified equations for concrete shells (Donnell equations of isotropic shells).

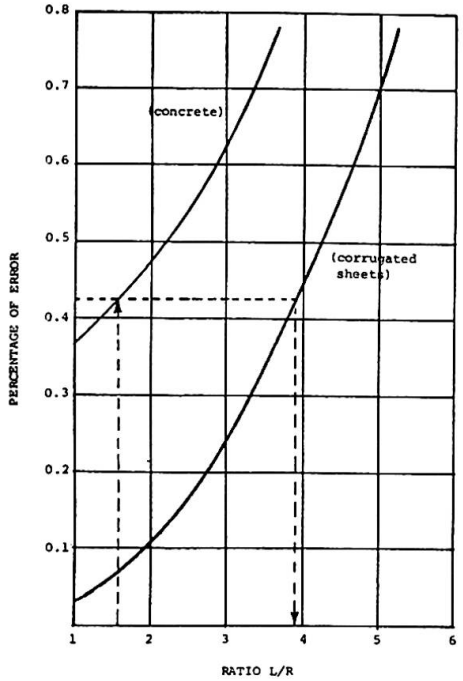

Fig. 2: Percentage of error in roots vs. the ratio L/R

The simplified Donnell equations are generally accepted for isotropic shells when $L/R < 1.6$ [5]. Fig. 2 shows that for $L/R < 3.9$, the same degree of approximation is not exceeded by using the simplified equations, Eqs. 3a, b, c for shells made of corrugated sheets.

BOUNDARY CONDITIONS

Three practical types of shells are analysed: I - shells with longitudinal stiffeners in the valleys only; II - shells with longitudinal stiffeners in valleys and crowns; III - half barrels supported along their four edges. Figs 3a, b, c show these three shells with the boundary conditions to each one of them.

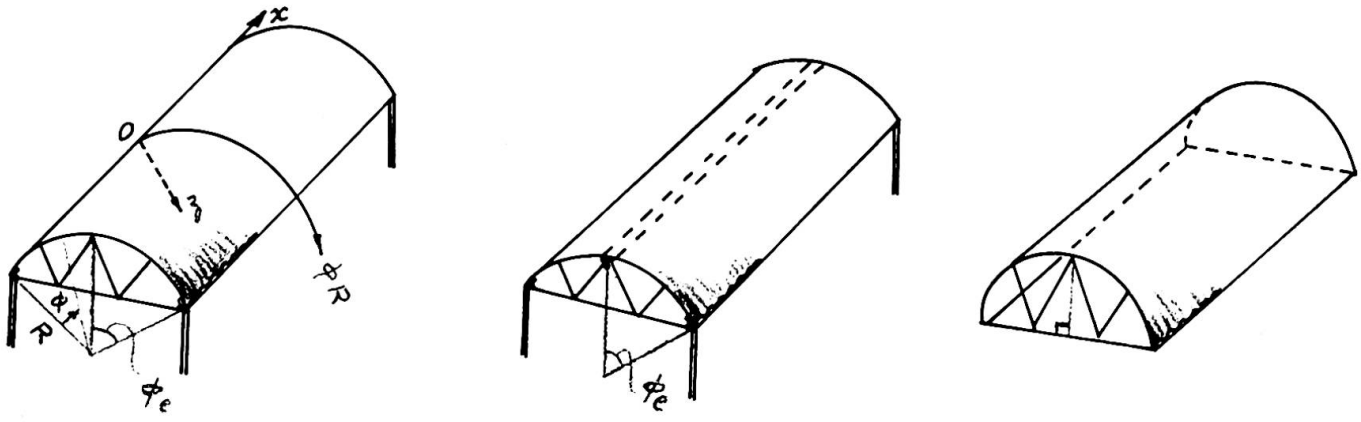

SHELL I

At $\phi = 0$ and $\phi = 2\phi_e$;

$M_\phi = 0$

$Q_\phi = 0$

$N_\phi = 0$

$\varepsilon_{x,shell} = \varepsilon_{x,stiffener}$

SHELL II

At $\phi = 0$, same as case I

At $\phi = \phi_e$;

$Q_\phi = 0$

$\theta = 0$

$v = 0$

$\varepsilon_{x,shell} = \varepsilon_{x,stiffener}$

SHELL III

At $\phi = 0$ and $\phi = 2\phi_e$

$w = 0$

$M_\phi = 0$

$v = 0$

$\varepsilon_x = 0$

Fig. 3: Types of Shells and Their Boundary Conditions

THEORETICAL RESULTS

The membrane and bending solutions are superimposed and the integration constants $A_n, B_n, \ldots$ of Eq. 10, are calculated for each type of shell satisfying the boundary conditions. In a similar way the displacements u and v are found and the components of internal forces are calculated and arranged in tables for practical use. These tables will be reported in reference [4].

COMPARISON BETWEEN THEORETICAL AND EXPERIMENTAL RESULTS

An experimental program was undertaken with full scale tests for the shells I and II, Fig. 3a, b. The experimental results show good agreement with those obtained theoretically. Fig. 4a, b, c are taken as a sample from the experimental program given in reference [4].

OBSERVATIONS AND CONCLUSIONS

1 - The theoretical analysis is verified experimentally. This proves that treating the corrugated sheets as orthotropic shells is a valid approach which adequately considers the main features of response of the shells.

2 - Design formulas and tables are prepared for practical use [4]. These formulas are based on the simplified governing equations, Eqs. 3a, b, c, which yield results with sufficient degrees of accuracy for shells with

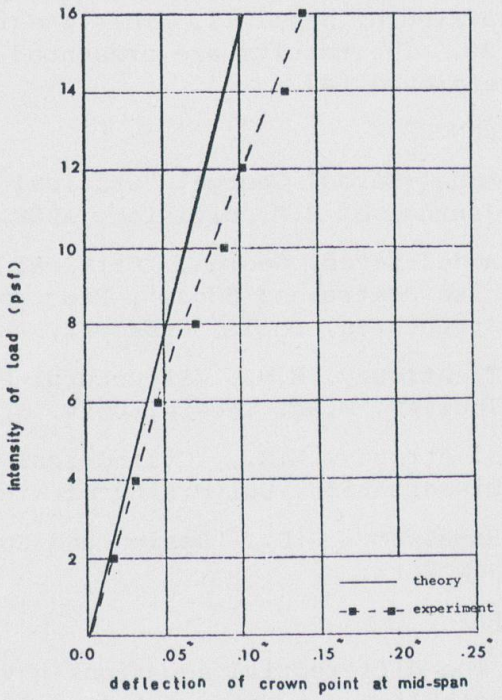

a - COMPARISON BETWEEN THEORETICAL AND EXPERIMENTAL LOAD-DEFLECTION CURVES OF CROWN POINT AT MID-SPAN.

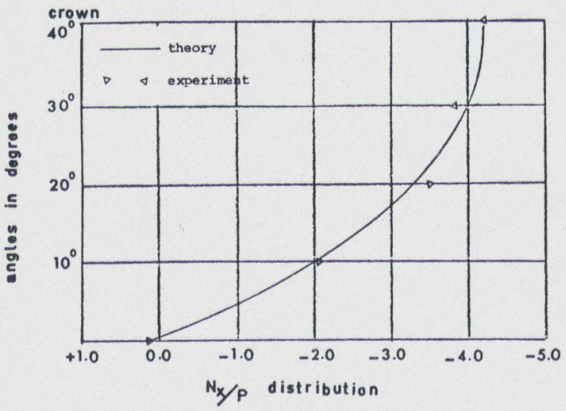

b - COMPARISON BETWEEN THEORETICAL AND EXPERIMENTAL VALUES OF N_x-DISTRIBUTION AT MID-SPAN.

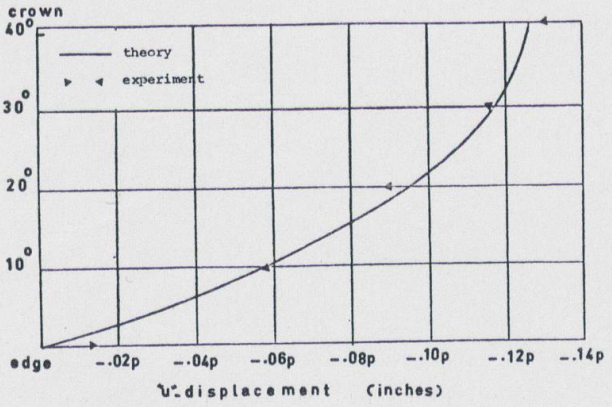

c - COMPARISON BETWEEN THEORETICAL AND EXPERIMENTAL VALUES OF THE DISPLACEMENT "U" AT SUPPORT.

Fig. 4: Comparison Between Experimental and Theoretical Results

the ratio $L/R \leq 3.9$. Shells with higher L/R ratios are handled as follows: a - Shell I undergoes too large deflections and becomes of no practical use; b - Shell II can be analysed as a beam. This approach yields results that are reasonably in agreement with the present analysis when $L/R \simeq 3.5$. Furthermore, the beam approach is expected to lead to better results for shells with higher ratios of L/R; c - The analysis of Shell III with $L/R > 3.9$ requires the use of the exact equations, Eq. 2a, b, c. This problem is

now under investigations.

3 - The local shear buckling is a prime factor in determining the ultimate load that can be carried by Shell II. This shear buckling was examined theoretically and experimentally [1, 2]. The results are presented in tables to supplement the design ones referred to in reference [4].

REFERENCES

1. Abdel-Sayed, George, "Critical Shear Loading of Curved Panels of Corrugated Sheets", Journal of E.M. Division, ASCE, Dec. 1970, pp. 895-912.

2. Abdel-Sayed, George, "Critical Shear Loading of Curved Panels of Corrugated Sheets With Restrained Edges", Proc. of the 1st Specialty Conference on Cold-Formed Steel Structures, Rolla, Missouri, Aug. 1971, pp. 167-172.

3. El-Atrouzy, M.N., "Structural Properties of Corrugated Sheets Used in Cylindrical Shells", M.Sc. Thesis, Univ. of Windsor, Windsor, Ontario, 1969.

4. El-Atrouzy, M.N., "Cylindrical Shell Roofs made of Corrugated Sheets", Ph.D. Dissertation, University of Windsor, (to be submitted in Sept. 1972).

5. Ramaswamy, G.S., "Design and Construction of Concrete Shell Roofs", McGraw-Hill, New York.

SUMMARY

The differential equations governing the behaviour of shells made of corrugated sheets are established in an exact as well as in a simplified form. The simplified equations yield acceptable results when the ratio of length to radius of the shell is less than 3.9. Membrane and bending solutions are superimposed to satisfy the governing equations as well as the boundary conditions.

An experimental program verified the theoretical results and showed that treating the corrugated sheets as orthotropic shells is an acceptable approach.

Double-Layer Space Frame Shells

Coupole à deux nappes et à treillis

Zweischichtige schalenförmige Rahmen

A. DI TOMMASO A. LA TEGOLA
Istituto di Tecnica delle Costruzioni
Facoltà di Ingegneria
University of Naples, Italy

Introduction: The double-layer reticulated shells are being used with increasing frequency to span large areas because they are less sensitive than single-layer shells to the progressive instability. The interest in prefabbricated units for these double-layer shells is growing constantly. In the first section of this paper we present some types of prefabbricated units of standard size and shape for these structures. In the second section we suggest a simple procedure for evaluating the collapse-load taking into account plasticity and post-buckling behaviour for reticulated structures. This evaluation is the main requirement for a minimum-weight design.

1,1) Units of standard size for double-layer reticulated shells

Let us think a plate subdivided in elementar cubes whose edges are equal to the plate thickness t (fig. 1A). This elementar cube can be divided in five tetrahedra (this is possible in two different ways). One of these tetrahedra is regular its edges measuring $t\sqrt{2}$, (fig. 1B). Let us consider, now, as first step, instead of each cube its fundamental tetrahedron defined by the condition that two connected tetrahedra have the upper (or lower) edge perpendicular each other. As second step we substitute to the compact tetrahedron a reticulated one consisting of six bars laying along the tetrahedron edges. In this manner we have a reticulated plate structure formed by reticulated tetrahedra. Now we note that if we eliminate from the reticulated tetrahedron two bars (those corresponding to the diagonals of opposite faces in the elementar cube) we obtain four bars in the position shown in fig. 1B. This is the standard unit, with rigid joints, that we call: "standard farfalla". In the fig. 1C we show the assembling of four standard units, while in the foto 1 (top-left) it appears a specimen in which have been assembled several units.

This "standard farfalla", with some small variations, can be utilized for generating several double-curved reticulated shells. A first solution can be obtained assembling two types of farfallas

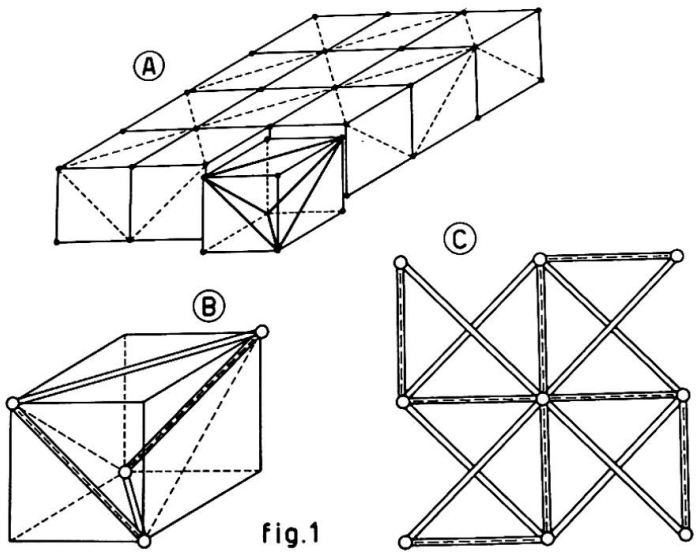

fig.1

one of which passess a bar shorter than the others, for generating double-layer cylindrical shells (foto 1 top-right).

The generation of a spherical double-curved shell starts from the truncated icosahedron inscript in a sphere (fig. 2a). This polihedron consists of 20 hexagons and 12 pentagons. Projecting the central points of these poligons on the spherical surface and connecting them with the vertexes of the corrispondent poligon, we obtain a triangulated net (fig. 2b) formed by 120+60 isosceles triangols of two types. Now we generate the double-layer spherical shell by four types of different farfallas (differents for side lenght), two of them having one side coincident with a side of two types of triangols. The other two are realized to complete the double-layer.

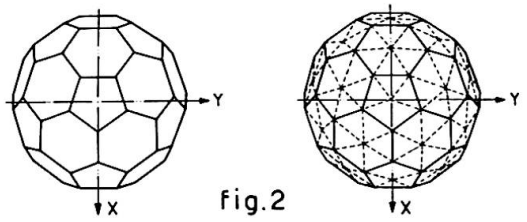

fig.2

A study for a connector of farfalla units is shown in foto 2.

II,1) Structural Analysis of reticulated structures

The main objective in the construction of reticulated structures is the employment of bars with equal section. The minimum-weight design requires the evaluation of the collapse load for a rational definition of the safety-factor. The procedures utilizing the limit-design teorems are unapplicable because these structures reach the collapse with bars in buckled configuration. Then the structural analysis must be conducted with "step by step" or "incremental" procedures. The relationship "axial force-elongation" N- (in tension and in compression) under the hypotesis of frictionless joints, represents tha basis for two approaches. The definition of this relationship is function of several parameters; this makes the practical application very arduous. For this reason it seems useful to define a simple N-ε law taking into account the plastic and unstable behaviour of bars.

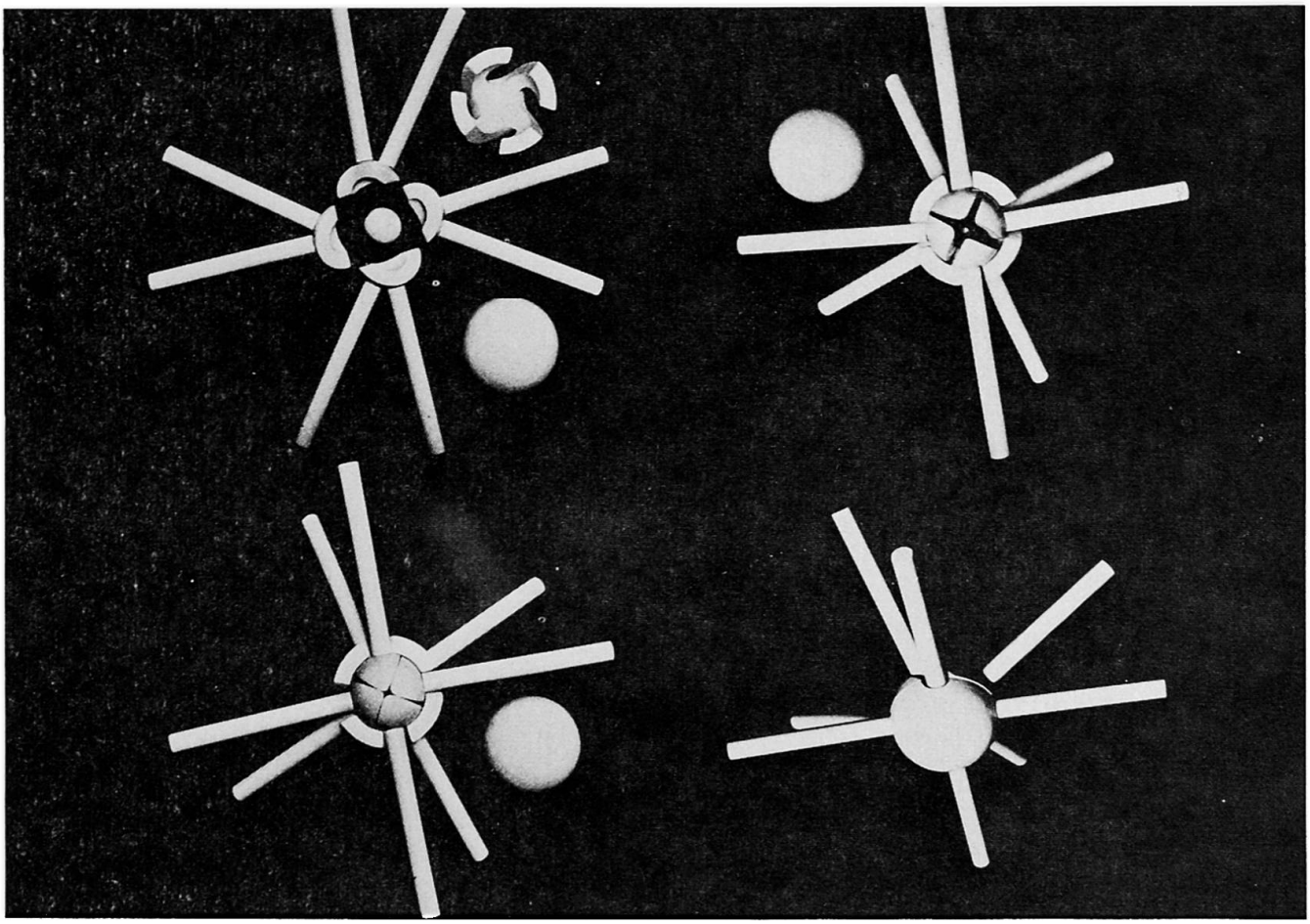

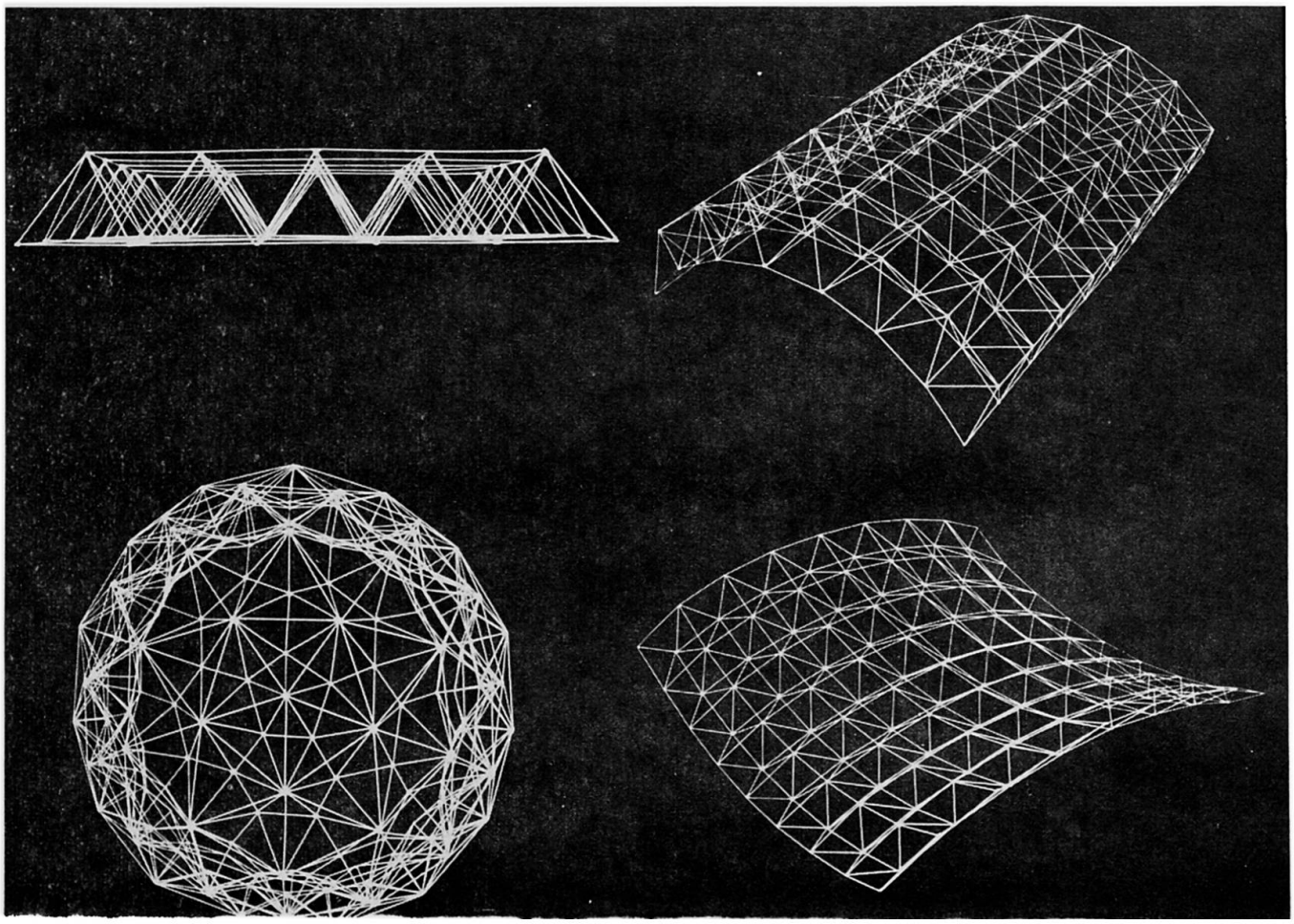

II,2) A simple N-ε relationship

Under the following hypotheses it is possible to define a simple N-ε relationship:

a) elastic-perfectly plastic behaviour of material,
b) bending moment-curvature with bilateral law,
c) yield function linearized,
d) deformability of bars localized in the middle section.

These hypotheses assure a prudent evaluation of the ultimate load. Indicating with N_o the limit axial force in tension and with M_o the limit bending moment, the linearized yield function is expressed by:

$$\Psi(M,N) = \pm \frac{N}{N_o} \pm \frac{M}{M_o} - 1 = 0 \qquad (1)$$

For the bars in compression the buckling axial load occurs for $N = N_{cr}$ in the elastic range that is before the bar reaches the limit axial force in compression $N = -N_o$. With the position $k = N/N_o$ and $k_{cr} = N_{cr}/N_o$ we have $-1 \leq k_{cr} \leq 0$, (fig. 3). For perfectly straight bars the lateral deflection of the middle section f will be zero before k reaches the condition $k/k_{cr} = 1$. According to the linear theory of stability and to elasto-plastic behaviour of material, the deflection f is indeterminate if $N = N_{cr}$ and $\Psi(M,N) \neq 0$. When $\Psi(M,N) = 0$ the deflection f is univocally determinate by (1) where we can consider $M = N\,f$. By putting $d = M_o/N_o$ the (1) can be written:

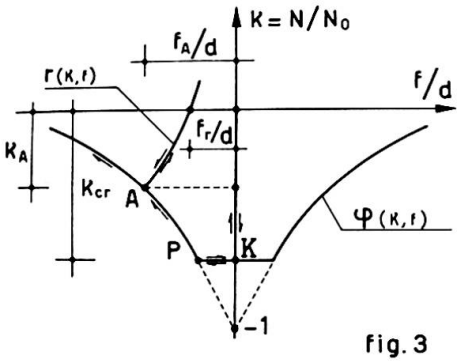

fig. 3

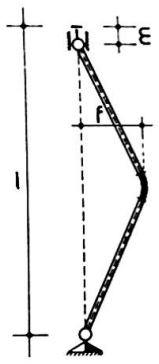

$$\varphi(k,f) = -k(1 \pm f/d) - 1 = 0 \qquad (2)$$

that in the (k, f/d) plane represents two branches of hyperbola (fig. 3).

Following the yield line $\varphi(k,f) = 0$, an increasing deflection f requires a reduction of $|N|$. Starting from a point A on the descending k-f/d branch, for a guided deflection, it is possible a decrease of the deflection's magnitude f ; the bar behaves elastically according to the law:

$$r\,(k,f) = \frac{k}{k_{cr}} + \left(1 - \frac{k_A}{k_{cr}}\right) \frac{f_A}{f} - 1 = 0 \qquad (3)$$

where f_A/d and k_A are the coordinates of the point A from which started the unloading process. Considering $N = 0$ that is $k = 0$ in (3), we obtain a "residual deflection" $f_r = f_A\,(1-k_A/k_{cr})$. The function r (k,f) represents a set of equilateral hyperbolas depending upon point A parameters, whose asymtotes are $k = k_{cr}$ and $f/d = 0$. For $A \equiv P$ (fig. 3) the hyperbola degenerates in its asymptotes. The "total elongation " is composed by two parts, the first depending on the elastic axial deformation, the second $(\Delta\ell/\ell)$ depending on the lateral deflection. The relationship $f - \Delta\ell$, under the previous hypotheses, is $\Delta\ell = 2\,f^2/\ell^2$. In fig. 4 we show the diagrams and the equations of these relationships.

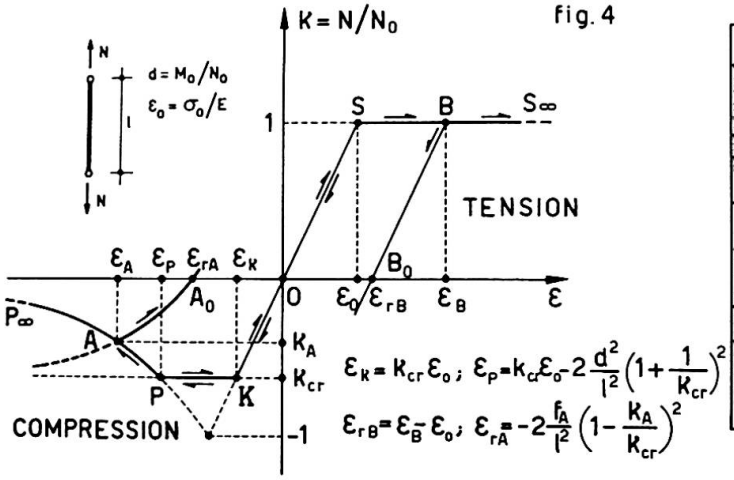

fig. 4

	BRANCH	K	ε	LAW	BEHAVIOUR
TENSION K>0	0-S	$0 \leq K < 1$	$0 \leq \varepsilon < \varepsilon_0$	$\varepsilon = K\varepsilon_0$	ELASTIC
	S-S∞	$K = 1$	$\dot{\varepsilon} = \frac{\dot{\mu}}{M_0} > 0$	$\dot{K} = 0$	PLASTIC
			$\dot{\varepsilon} < 0$	$\dot{K} = \dot{\varepsilon}/\varepsilon_0$	ELASTIC
	B-B₀	$0 \leq K < 1$	$\varepsilon_{rB} \leq \varepsilon < \varepsilon_B$	$K = \frac{\varepsilon - \varepsilon_{rB}}{\varepsilon_0}$	ELASTIC
COMPRESSION K<0	0-K	$K_{cr} < K \leq 0$	$\varepsilon_K < \varepsilon \leq 0$	$\varepsilon = K\varepsilon_0$	ELASTIC
	K-P	$K = K_{cr}$	$\varepsilon_P \leq \varepsilon \leq \varepsilon_K$	$\dot{K} = 0$	ELASTIC (NEUTRAL EQ.)
	P-P∞	$0 \leq K \leq K_{cr}$	$\varepsilon < \varepsilon_P$, $\dot{\varepsilon} < 0$	$\varepsilon = K\varepsilon_0 - 2\frac{d^2}{l^2}\left(1+\frac{1}{K}\right)^2$	PLASTIC (INSTABLE EQ.)
			$\varepsilon < \varepsilon_P$, $\dot{\varepsilon} < 0$	$\varepsilon = K\varepsilon_0 + \varepsilon_{rA}\left(1-\frac{K}{K_{cr}}\right)^2$	ELASTIC
	A-A₀	$0 \leq K \leq K_{cr}$	$\varepsilon \geq \varepsilon_A$		ELASTIC (STABLE EQ.)

Then the structural analysis can be performed, for each load increment, by the definition of the corresponding behaviour of every bar depending on the position of the representative point in the diagram of fig. 4. This procedure, repeated for successive finite load increments, leads to the evaluation of the collapse-load.

II,3) Numerical example

To clarify the method proposed for the evaluation of the collapse-load for reticulated structures we consider here the simple example shown in fig. 5.

The equilibrium and compatibility equations are:

$$N^A - N^B - F = 0 \qquad (4a)$$

$$\mathcal{E}^A + 2\,\mathcal{E}^B = 0 \qquad (4b)$$

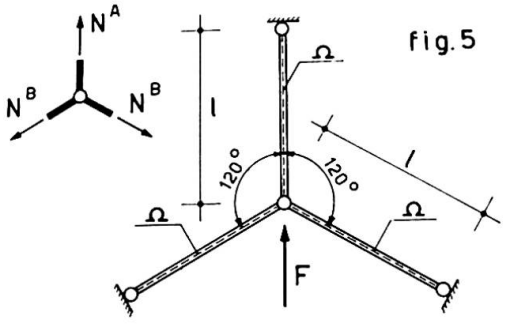

fig. 5

In the elastic field the axial forces are: $N^A = -2F/3$; $N^B = F/3$. Being $|N^A| > |N^B|$ the load increment leads to point K (fig. 4) where is $\mathcal{E}^A = k_{cr}\,\mathcal{E}_o$. The corresponding value of the external force is $F_K = -1{,}5\ k_{cr}\ N_o$. Further external load increments will correspond to constant axial forces in the bar A (K P branch in fig. 4) while the representative point on the N- diagram will reach the point P for the bar A or the point S for the bar B.

In the case:

$$-2\,\mathcal{E}_o \geq k_{cr}\,\mathcal{E}_o - 2\,\frac{d^2}{\ell^2}\,(1 + \frac{1}{k_{cr}})^2 \qquad (5)$$

the point S will be reached before or simultaneously to the point P. Then the structure can't bear further load increments because beyond the point P and S the force in the tension bars remains constant while the force in the compressed bear must have a reduction (in absolute value). The limit load in this case is $F'_\ell = N_o\,(1-k_{cr})$.

In the other case, if the (5) is unsatisfied the compressed bar will reach the point P before the tension bars reach the point S. The internal force in the compressed bar must have a reduction in absolute value, while in the tension bars the force can have an increment as far as the point S will be reached. The compatibility equation (4b) allows to joint the deformation of the three bars, by putting $\varepsilon^A = -2\ \varepsilon_o$ we obtain the axial force in the bar A while in tension bars the force is equal to N_o. The limit load is:

$$F''_\ell = N_o - (-2\ \varepsilon_o)\ N^A \qquad (6)$$

If the three bars have a tubular section whose diameter is D and tickness t, indicating with λ the slenderness, we have:

$$k_{cr} = -\frac{\pi^2}{\lambda^2}\ \frac{1}{\varepsilon_o}\ ; \qquad \frac{\ell}{d} = \frac{\sqrt{2}}{4}\ \pi\lambda \qquad (7)$$

being $\lambda = \ell/\varrho = 2\ \sqrt{2}\ \ell/D$. Assuming $\varepsilon_o = 2\times10^{-3}$, $\lambda = 100$ we have:

$$F_k = 0{,}74\ N_o\ ; \quad F''_\ell = 1{,}17\ N_o\ ; \quad F''_\ell/F_k \cong 1{,}59$$

where F_k is the external force corresponding to compressed member instability and F''_ℓ is the collapse-load.

REFERENCES

[1] CERADINI, G. — Strutture reticolari iperstatiche Costruzioni Metalliche n° 3, 1965

[2] DE DONATO, O. — Legami forze-elongazioni per aste compresse in fase post-critica. Rend. Ist. Lomb. Sci. Lett. vol. 99, 1965

[3] MAIER, G. — Behaviour of elastic plastic trusses with unstable bars. - Journal of the Engineering Mechanics Division - ASCE vol. 93, 1966

[4] DE DONATO, O. — Legami forze-elongazioni per aste elasto-plastiche compresse ad elongazione decrescente. Rend. Ist. Lomb. Sci. Lett. - vol. 100, 1966

[5] MAIER, G. DRUCKER, D.C. — Elastic-plastic continua containing unstable elements obeying normality and convexity relations. - Schweizerischen Bauzeitung - vol. 84, n° 23, 1966

SUMMARY: In this paper we show a solution for the construction of double-layer space frame shells with simple prefabbricated units of standard size and shape. Then a procedure is proposed for the evaluation of the actual safety-factor by means of the calculation of the collapse-load of these structures taking into account plasticity and local buckling of simple bars.